

Rotons and Solitons in Dynamical Phyllotaxis

Cristiano Nisoli, Paul E. Lammert and Vincent H. Crespi

Department of Physics, The Pennsylvania State University, University Park, PA 16802-6300

(Dated: January 23, 2019)

Multiple rotons and a large family of topological solitons that can fragment, merge and interconvert upon collision arise when particles with a generic repulsive interaction experience a dimensional mismatch: if a one-dimensional lattice is wrapped helically onto a cylinder, the nearest neighbors along the lattice are no longer nearest neighbors in three dimensional space.

PACS numbers: 63.22.+m, 87.10.+e, 68.65.-k, 89.75.Fb

A complete physical system typically requires three elements: particle, interaction, and manifold. Condensed matter physics provides a rich framework for generating new effective particles and new interactions such as quasiparticles, Cooper pairs or composite fermions. Rather than generate new effective particles or interactions within familiar flat space, one can also ask how novel geometrical constraints on the underlying manifold can generate new physics, even for old familiar interactions [1, 2]. Perhaps the simplest effective interaction is a featureless long-ranged repulsion. Classical repulsive particles in flat space assume simple structures: in two dimensions, a triangular Wigner lattice. In contrast, interacting repulsive particles on a cylinder generate a rich family of helical structures that follow Fibonacci rules first seen in phyllotaxis, the study of plant morphology [3, 4, 5]. Since the mathematical patterns of phyllotaxis require only a generic repulsive interaction, they appear in a wide variety of fields, including biochemistry [4, 6] fluid dynamics [7], magnetism [8], elasticity [9], superconductivity [5] and beam physics [10, 11].

Classic botanical phyllotactic systems such as cacti do not possess dynamics (aside from slow growth), but alternative physical realizations can show dynamical phenomena. Here we demonstrate that the linear dynamics of phyllotaxis generates rotons and the nonlinear regime supports a large family of dynamically stable topological solitons that can fragment, merge, or interconvert upon collision, with propagation speeds governed by energy conservation and phase matching. These new phenomena should be observable in a wide range of systems, from quantum to classical and from nanometer-scale to macroscopic.

To describe phyllotaxis, we assume a Bravais lattice structure in one dimension, wrapped helically (with an axial spacing a) onto a cylinder of radius R , as shown in Fig. 1. At a given density this lattice is described by a single parameter Ω , the screw angle between successive particles. For a generic pair-wise repulsive interaction v_{ij} between particles i and j , the energy of the static lattice is $V = \frac{1}{2} \sum_{i \neq j} v_{i,j}$. Since the lattice structure is defined by Ω , we can write $V(\Omega)$. The lowest-energy spiral at low density (i.e. large a/R) has $\Omega = \pi$, since that angle generates the largest inter-particle separation. At

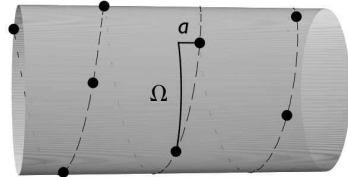


FIG. 1: Repulsive particles arrayed along a one-dimensional Bravais lattice wrapped onto the surface of a cylinder. a is the axial separation between particles and Ω is the screw angle.

a slightly higher density, the second neighbor according to the Bravais lattice becomes the first neighbor in real space, and the angle π becomes unfavorable. As a/R decreases, the number of maxima in $V(\Omega)$, increases. For a/R low enough, any commensurate spiral of screw angle $\Omega = 2\pi i/j$ with i, j relatively prime becomes a local maximum, called a peak of rank j , as in Fig 2.

The degeneracy of $V(\Omega)$ will be important to the dynamics of solitons, so we develop it here. Peaks of equal rank are nearly degenerate, since their principal defining energetic contribution arises from particles facing each other at a distance ja . The minima also become more nearly degenerate as the density increases, since for angles incommensurate to π each particle is embedded in a nearly uniform background charge from the other particles. We can relate the degeneracies of both minima and maxima to purely geometrical parameters. Grouping peaks into families of equal rank $P_j \equiv \{\Omega = 2\pi i/j \mid \text{for } i, j \text{ coprime and } i \leq j\}$ generates a Farey class of order j , i.e. all fractions in lowest terms between 0 and 1 whose denominators do not exceed j [12]. The cardinality of P_j is Euler's totient function, $\phi(j)$ [13]. The degeneracy D of the energy minima for a system with a maximum peak rank J is then [13]

$$D = \sum_{j=1}^J \phi(j) = \frac{3}{\pi^2} J^2 + O(J \log J), \quad (1)$$

which scales as $D \sim 2R/a$: new peaks of rank J appear at $\Omega = 2\pi i/J$ (i, J coprime) when the distance (in three-dimensional space) between particles separated axially by a equals that between particles separated axially by

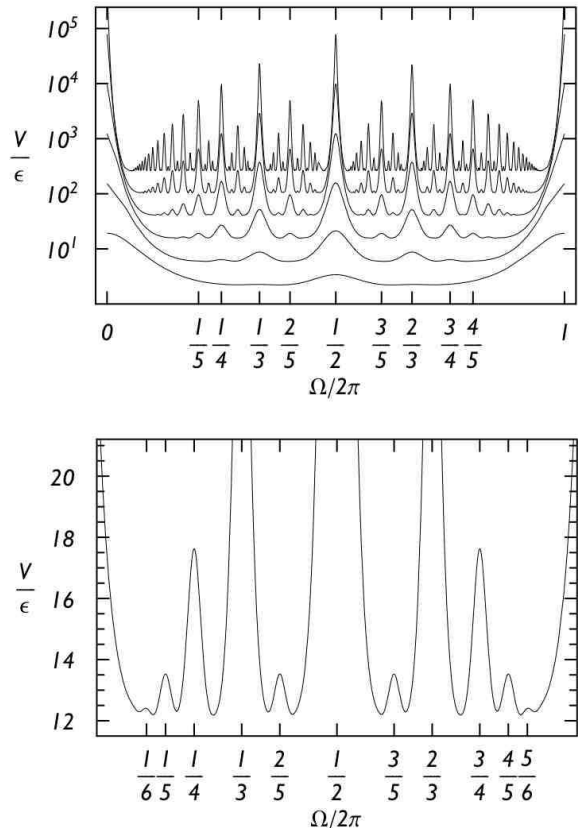


FIG. 2: Lattice energy $V(\Omega)$ versus screw angle for successively halving values of a/R starting from 0.5 (top), and in detail for $a/R = 0.15$ (bottom). The highest rank observed, $J = 6$, matches Eq. 2.

Ja . For reasonably large values of J ,

$$J = \left[\left[\sqrt{\frac{2\pi R}{a}} \right] \right], \quad (2)$$

where $\left[\left[\right] \right]$ denotes the integer part. A minimum in $V(\Omega)$ bracketed by peaks of rank j_1 and j_2 corresponds to a rhombic lattice where each particle has its nearest neighbors at axial displacements of $\pm aj_1$, $\pm aj_2$ and second nearest neighbors at $\pm a(j_1 + j_2)$ or $\pm a(j_1 - j_2)$ [5]. The so-called parastichy numbers j_1 and j_2 give the number of crossing secondary spirals (parastichies) needed to cover the lattice by connecting nearest neighbors.

To study dynamics, we constrain the particles to fixed axial positions ia , leaving the angular coordinates θ_i as dynamical variables. The resulting excitations are similar to the transverse modes of an axially unconstrained system. The total energy is

$$E = \frac{1}{2} I \sum_i \dot{\theta}_i^2 + V. \quad (3)$$

For specificity, we take the particles as dipoles \mathbf{p} directed radially outward [14], but the essential results apply to any reasonably smooth and long-ranged potential. The

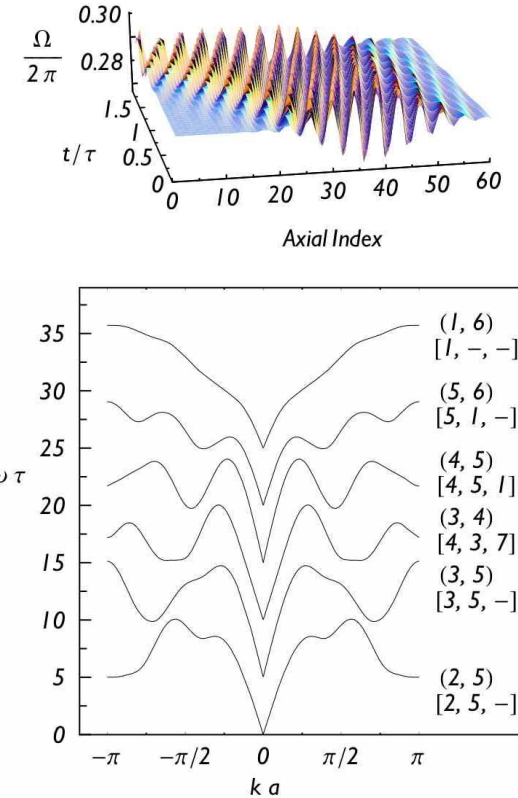


FIG. 3: Phonon dispersion relations for the structures in the lower panel of Fig. 2, each spectrum offset by $5 T^{-1}$ for clarity. Corresponding parastichy numbers (j_1, j_2) and nearest three neighbors $[\tilde{j}_1, \tilde{j}_2, \tilde{j}_3]$ with $(\omega_1 \tilde{j}_1 > \omega_2 \tilde{j}_2 > \omega_3 \tilde{j}_3)$ are given. The simple estimate for the number of rotons and maxons, $2\tilde{j}_1 - 1$, holds for all but (2,5). The upper panel shows a wave-packet centered at $ka = 1.5$ for the structure with parastichy numbers (3, 4).

natural energy and frequency scales are $\epsilon = p^2 R^{-3}$ and $\tau = \epsilon^{-1/2} I^{1/2}$.

Consider oscillations $\theta_n = \bar{\Omega}n + \psi_n(t)$, around a stable structure $\bar{\Omega}$, with normal modes $\psi_n(t) = \Psi_k \cos[kn - \omega(k)t]$. The most important interactions are between nearest neighbors in space, which generally are *not* nearest neighbors on the underlying one-dimensional Bravais lattice. Thus, we express the frequency as

$$\omega(k)^2 = 2\omega_{j_1}^2 [1 - \cos(j_1 k)] + 2\omega_{j_2}^2 [1 - \cos(j_2 k)] + \dots \quad (4)$$

where j_m is the relative index of the m -th neighbor (e.g., $j_1 = 4$ for the (4, 5) structure) and ω_m is proportional to the second derivative of $v_{0,m}$ at the equilibrium positions defined by $\bar{\Omega}$. The wave-number k ranges in the interval $[-\pi, \pi]$, which is *not* a Brillouin zone for our (axially aperiodic) lattice. Fig. 3 shows the dispersion relations for the stable structures in the lower panel of Fig. 2, truncating Eq. (4) to 25 terms. The dispersion is highly non-monotonic outside of the long-wavelength acoustic regime. To gain insight into the origin of the multiple extrema, consider retaining only contributions from nearest

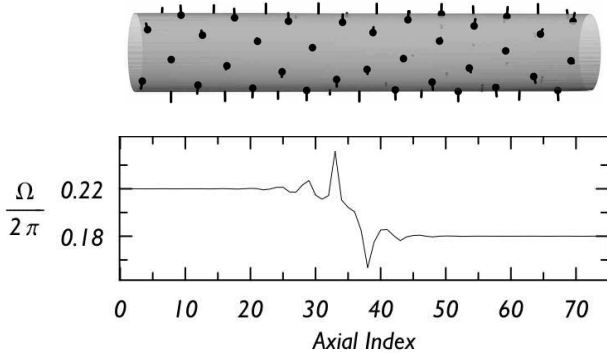


FIG. 4: A kink between domains of parastichy numbers (4,5) and (5,6) as it appears on the physical cylinder and in a plot of the angular shift Ω versus the axial index.

neighbors, and label them so that $\omega_{j_1 j_1} > \omega_{j_2 j_2}$. Since (j_1, j_2) are parastichy numbers for $\bar{\Omega}$, they are relatively prime. Therefore the dispersion relation in this approximation has no period smaller than 2π , but generally contains multiple local extrema. The nearest-neighbor approximation predicts the number of rotonic and maxonic extrema to be $2j_1 - 1$.

Rotons in helium are density fluctuations whose unusual dispersion relation has often been ascribed to an intrinsically quantum mechanical origin [15]. By contrast, phyllotactic rotons are entirely classical and do not involve density fluctuations, since the particles have fixed axial positions. These rotons arise because nearest neighbors along the underlying one-dimensional spiraling Bravais lattice are not necessarily nearest neighbors in three-dimensional space: although increasing wave-vector drives particles nearby *along the spiral* increasingly out of phase, it can drive particles that are neighbors *in three dimensional space* more nearly into phase. An integration of the full equations of motion, shown in Fig. 3, verifies rotonic behavior and demonstrates the dynamical stability of the lattice under small perturbations.

Thermodynamically, this highly degenerate one-dimensional system should be unstable towards domain-wall formation. Static step-like kinks, imposed as an initial condition, radiate energy in the form of traveling waves; when the resulting configurations are temporally averaged to remove residual oscillations and then used as new initial conditions, the resulting kink is static, as shown in Fig. 4. These kinks are not particular to the dipolar interaction: simulations of cooled ion beams also show numerous kinks in the outer ion shell [10].

These kinks can travel and maintain shape as solitons. Since a kink separates domains of different screw angle, its motion must be accompanied by either phase slips or a uniform relative rotation of the two domains. The latter, adiabatic, motion is observed. Unlike other topological solitons such as the sine-Gordon variety, which can travel at any subsonic speed, here the speed of the kink, v_K , is tightly controlled by the dual constraints of energy con-

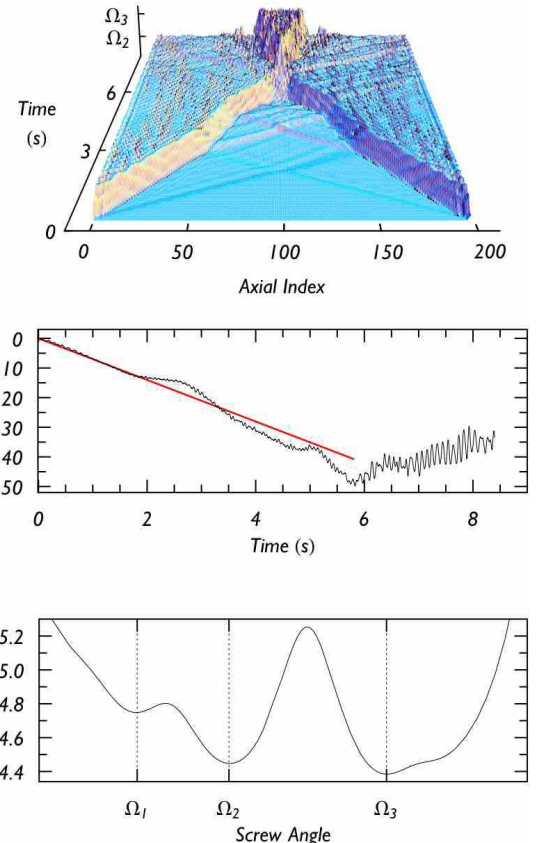


FIG. 5: The collision of two solitons. For clarity, weak high-wave-vector phonons were smoothed by spatial averaging, here and in Fig. 6. The potential energy V drops linearly as the lower-energy domains advance; deviations starting around $t = 2$ arise from interaction with elastic waves propagating in front of the solitons. The energy $V(\Omega)$ reflects an actual experimental apparatus of magnets and bearings, with $a/R = 0.7$ and minima at $\Omega_1/2\pi = 0.23$, $\Omega_2/2\pi = 0.28$, $\Omega_3/2\pi = 0.38$. An animation is available online [18].

servation and phase matching at the interface between the two domains. Fig. 5 shows a pair of solitons that form at the free ends of an initially stationary metastable structure Ω_1 in a low-density system with non-degenerate minima. As the solitons move toward each other, (preceded by elastic waves to ensure local angular momentum conservation [16]), lower-energy domains of angle Ω_2 form in their wakes. The angular speed of the Ω_2 domains is $\dot{\theta} = v_K \Delta \Omega$, where $\Delta \Omega = \Omega_2 - \Omega_1$. Approximating the kink as a step, the time dependent energy is $E(t) = (I \Delta \Omega^2 v_k^2 - 2\Delta V) v_K t$, where $\Delta V > 0$ is the potential energy gained by a particle upon transfer from the outer (Ω_2) to the inner (Ω_1) domain [17]. Energy conservation then fixes v_K :

$$v_K^2 = \frac{2\Delta V}{I \Delta \Omega^2}. \quad (5)$$

For the simulation of Fig. 5, the measured speed 22.1 s^{-1} agrees well with the value predicted from Eq. 5, 23.4 s^{-1} .

More general simulations of interacting solitons exhibit

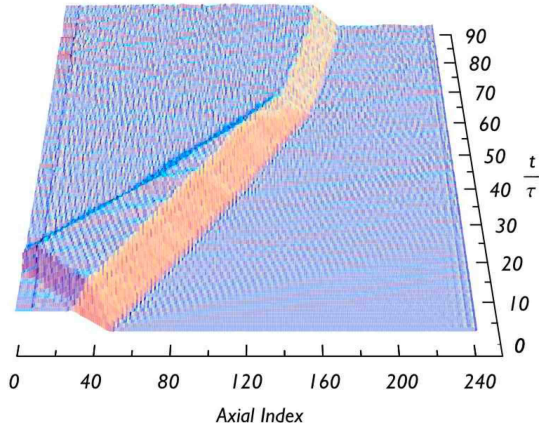


FIG. 6: Fragmentation, reflection and merger of solitons for a system with $a/R = 0.15$, as in Fig. 2. An animation is available online [18].

a complex phenomenology [19]. Solitons can convert from one species to another upon collision, as seen at later times in Fig. 5. At low densities, unstable domain boundaries can spontaneously fragment into pairs of counter-propagating solitons. Two different solitons moving in the same direction at different speeds can merge to form a third soliton. Fig. 6 demonstrates the latter phenomenon. Initial conditions are prepared so that two solitons emerge from an initial domain boundary. The left-hand soliton bounces off the free left-hand boundary, maintains its shape, and propagates rightward faster than the other. The two solitons then collide, merge and transform in a third soliton with a different characteristic speed. This set of behaviors is strikingly reminiscent of particle physics: like elementary particles, phyllotactic solitons can merge, split, decay and change identity upon collision. At sufficiently high temperature, they decompose into a sea of constituent particles. Both hadrons and phyllotactic solitons provide a family of quasi-degenerate, dynamically stable, composite objects. This similarity does not seem to rise beyond the level of a interesting analogy, however.

Since these results generalize to any long-ranged repulsive interaction, many cylindrically symmetric systems could support dynamical phyllotaxis. Cold atomic gases, with their extremely low dissipation, are particularly attractive. Adatoms [20] or low-density electrons on carbon or boron nitride nanotubes could provide an example in condensed matter physics, and cooled particle beams provide an opportunity in particle physics. Colloidal particles in mesophase systems, which can self-assemble in cylindrical geometries [21], could provide a more strongly damped version, and constrained magnets [22] a macroscopic one. A two-dimensional Wigner crystal forms when $r_s > 37$ [23]. To achieve phyllotactic degeneracy, $a/R = r_s^2/2R^2$ must be small enough. At $r_s = 37$, Eq. 2

requires a minimal radius

$$R \geq \frac{37J}{2\sqrt{\pi}}a_0 \simeq 5.5J \text{ \AA} \quad (6)$$

to generate a maximum peak rank J , with a_0 the Bohr radius for an appropriate effective mass and dielectric constant. When $a_0 = 0.53 \text{ \AA}$, the minimal degeneracy, $D = 2$ and $J = 2$, occurs for $R \simeq 11 \text{ \AA}$, a typical dimension for a carbon or boron nitride nanostructure. Axial relaxation of particle positions in a real Wigner crystal changes the particle density inside the kink [16], suggesting the possibility of charge transport via these solitons in a pinned crystal, if enough translational order survives [24].

In conclusion, repulsive classical particles, when constrained to a cylindrical shell, generate a new class of phyllotactic rotons and inter-converting protean solitons. This work was supported by the National Science Foundation through grants DMR-0305035, DMR-0609243 and ECS-0609243.

- [1] J. J. Thomson, *Philos. Mag.* **7**, 237 (1904).
- [2] A. R. Bausch, M. J. Bowick, A. Cacciuto, A. D. Dinsmore, M. F. Hsu, D. R. Nelson, M. G. Nikolaides, A. Travesset and D. A. Weitz, *Science* **299**, 1716 (2003).
- [3] A. W. Thompson, *On Growth and Form*, Cambridge Univ. Press, NY, 1959 (first edition 1917); R. V. Jean, *Phyllotaxis: a Systemic Study in Plant Morphogenesis*, Cambridge Univ. Press, Cambridge 1994. <http://maven.smith.edu/~phylo/> provides an overview.
- [4] I. Adler, D. Barabe and R. V. Jean, *Ann. Bot. London* **80**, 231 (1997).
- [5] S. L. Levitov, *Phys. Rev. Lett.* **66**, 224 (1991); S. L. Levitov, *EuroPhys. Lett.* **14**, 533 (1991).
- [6] A. Frey-Wyssling *Nature* **173**, 596 (1954); R. O. Erickson *Science* **181**, 705 (1973)
- [7] N. Rivier, R. Ocelli, J. Pantaloni and A. Lissowski, *J. Phys.* **45**, 49 (1984).
- [8] S. Douady and Y. Couder, *Phys. Rev. Lett.* **68**, 2098 (1992).
- [9] P. D. Shipman and A. C. Newell, *Phys. Rev. Lett.* **92**, 168102 (2004); C. Li, X. Zhang, Z. Cao, *Science* **209**, 909 (2005).
- [10] A. Rahman and J. P. Schiffer *Phys. Rev. Lett.* **57**, 1133 (1986).
- [11] T. Shatz, U. Schramm, D. Habs, *Nature* **412**, 717 (2001); U. Schramm, T. Shatz, D. Habs, *Phys. Rev. E* **66**, 036501 (2002).
- [12] J. Farey, *London, Edinburgh and Dublin Phil. Mag.* **47**, 385 (1816).
- [13] J. H. Conway, and R. K. Guy, *The Book of Numbers* (Springer-Verlag, New York, 1996); T. Nagell, *Introduction to Number Theory* (Wiley, New York, 1951).
- [14] Their interaction is repulsive at the densities studied.
- [15] R. Donnelly, *Phys. World* **10**, 25 (1997); R. P. Feynman and M. Cohen, *Phys. Rev.* **102**, 1189 (1956).
- [16] C. Nisoli and V. H. Crespi, in preparation.
- [17] Energy associated with elastic waves that precede the solitons must also be included in ΔV and $\Delta\Omega$.

- [18] See EPAPS Document No. [??] for animations of the soliton collisions. For more information on EPAPS, see <http://www.aip.org/pubservs/epaps.html>.
- [19] F. D. Tappert and N. J. Zabusky, Phys. Rev. Lett. **27**, 1774 (1971).
- [20] Widely separated K atoms (~ 60 Å) on graphite have a repulsive dipole-dipole interaction. Z. Y. Li, K. M. Hock and R. E. Palmer Phys. Rev. Lett. **67**, 1562 (1991); R. D. Diehl, R. McGrath Surf. Sci. Rep. **23** 43 (1996).
- [21] D. J. Pochan, Z. Chen, H. Cui, K. Hales, K. Qi, K. L. Wooley, Science **306**, 94 (2004) and references therein.
- [22] J. Stambaugh, D. P. Lathrop, E. Ott and W. Losert, Phys. Rev. E **68**, 026207 (2003).
- [23] B. Tanatar and D. M. Ceperley, Phys. Rev. B **39**, 5005 (1989).
- [24] R. Chitra, T. Gianmarchi and P. Le Doussal, Phys. Rev. B **65**, 035312 (2001).